

Effect of Proximity of Sheet Pile Walls on the Apparent Capacity of Driven Displacement Piles, Phase 2: Final Report Task 3 Deliverable

May 2019

Sponsor:

Florida Department of
Transportation (FDOT)

Project Manager:

Juan Castellanos

Principal Investigator:

Ted Krauthammer, Ph.D.

Jae H. Chung, Ph.D.

Research Assistants:

Nikhil Mishra, Adam Taylor

Address:

Engineering School of
Sustainable Infrastructure and
Environment (ESSIE)
College of Engineering
University of Florida (UF)
1949 Stadium Rd. Room 365
Gainesville FL 32611

Project Number:

BDV31 TWO 977-102

DISCLAIMER

The opinions, findings, and conclusions expressed in this publication are those of the authors and not necessarily those of the State of Florida Department of Transportation.

SI (MODERN METRIC) CONVERSION FACTORS (FROM FHWA)

APPROXIMATE CONVERSIONS TO SI UNITS

SYMBOL	WHEN YOU KNOW	MULTIPLY BY	TO FIND	SYMBOL
LENGTH				
in	inches	25.4	millimeters	mm
ft	feet	0.305	meters	m
yd	yards	0.914	meters	m
mi	miles	1.61	kilometers	km

SYMBOL	WHEN YOU KNOW	MULTIPLY BY	TO FIND	SYMBOL
AREA				
in²	square inches	645.2	square millimeters	mm ²
ft²	square feet	0.093	square meters	m ²
yd²	square yard	0.836	square meters	m ²
mi²	square miles	2.59	square kilometers	km ²

SYMBOL	WHEN YOU KNOW	MULTIPLY BY	TO FIND	SYMBOL
VOLUME				
fl oz	fluid ounces	29.57	milliliters	mL
ft³	cubic feet	0.028	cubic meters	m ³
yd³	cubic yards	0.765	cubic meters	m ³

NOTE: volumes greater than 1,000 L shall be shown in m³

SYMBOL	WHEN YOU KNOW	MULTIPLY BY	TO FIND	SYMBOL
MASS				
oz	ounces	28.35	grams	g
lb	pounds	0.454	kilograms	kg
T	short tons (2,000 lb)	0.907	megagrams (or "metric ton")	Mg (or "t")

SYMBOL	WHEN YOU KNOW	MULTIPLY BY	TO FIND	SYMBOL
TEMPERATURE (exact degrees)				
°F	Fahrenheit	5 or (F-32)/1.8	(F-32)/9 Celsius	°C

SYMBOL	WHEN YOU KNOW	MULTIPLY BY	TO FIND	SYMBOL
ILLUMINATION				
fc	foot-candles	10.76	lux	lx
fl	foot-Lamberts	3.426	candela/m ²	cd/m ²

SYMBOL	WHEN YOU KNOW	MULTIPLY BY	TO FIND	SYMBOL
FORCE and PRESSURE or STRESS				
lbf	pound force	4.45	newtons	N
kips	kips	4,448.22	newtons	N
lbf/in²	pound force per square inch	6.89	kilopascals	kPa
ksi	kips per square inch	6,894.76	kilopascals	kPa
tsf	tons (short) per square foot	95.67	kilopascals	kPa
pcf	pound force per cubic foot	156.967	newtons per cubic meter	N/m ³

APPROXIMATE CONVERSIONS TO SI UNITS

SYMBOL	WHEN YOU KNOW	MULTIPLY BY	TO FIND	SYMBOL
LENGTH				
mm	millimeters	0.039	inches	in
m	meters	3.28	feet	ft
m	meters	1.09	yards	yd
km	kilometers	0.621	miles	mi

SYMBOL	WHEN YOU KNOW	MULTIPLY BY	TO FIND	SYMBOL
AREA				
mm ²	square millimeters	0.0016	square inches	in ²
m ²	square meters	10.764	square feet	ft ²
m ²	square meters	1.195	square yards	yd ²
ha	hectares	2.47	acres	ac
km ²	square kilometers	0.386	square miles	mi ²

SYMBOL	WHEN YOU KNOW	MULTIPLY BY	TO FIND	SYMBOL
VOLUME				
mL	milliliters	0.034	fluid ounces	fl oz
L	liters	0.264	gallons	gal
m ³	cubic meters	35.314	cubic feet	ft ³
m ³	cubic meters	1.307	cubic yards	yd ³

SYMBOL	WHEN YOU KNOW	MULTIPLY BY	TO FIND	SYMBOL
MASS				
g	grams	0.035	ounces	oz
kg	kilograms	2.202	pounds	lb
Mg (or "t")	megagrams (or "metric ton")	1.103	short tons (2,000 lb)	T

SYMBOL	WHEN YOU KNOW	MULTIPLY BY	TO FIND	SYMBOL
TEMPERATURE (exact degrees)				
°C	Celsius	1.8C+32	Fahrenheit	°F

SYMBOL	WHEN YOU KNOW	MULTIPLY BY	TO FIND	SYMBOL
ILLUMINATION				
lx	lux	0.0929	foot-candles	fc
cd/m ²	candela/m ²	0.2919	foot-Lamberts	fl

SYMBOL	WHEN YOU KNOW	MULTIPLY BY	TO FIND	SYMBOL
FORCE and PRESSURE or STRESS				
N	newtons	0.225	pound force	lbf
N	newtons	0.000224809	kips	kips
kPa	kilopascals	0.145	pound force per square inch	lbf/in ²
kPa	kilopascals	0.000145	kips per square inch	ksi
kPa	kilopascals	0.000145038	kips per square inch	ksi
N/m ³	newtons per cubic meter	0.0104526	pound force per cubic foot	pcf

*SI is the symbol for International System of Units. Appropriate rounding should be made to comply with Sec. 4 of ASTM E380. (Revised March 2003)

1. Report No.	2. Government Accession No.	3. Recipient's Catalog No.	
4. Title and Subtitle Effect of Proximity of Sheet Pile Walls on the Apparent Capacity of Driven Displacement Piles, Phase 2		5. Report Date May 2019	
		6. Performing Organization Code	
7. Author(s) Chung, J., Krauthammer, T., Mishra, N., Taylor, A.		8. Performing Organization Report No.	
9. Performing Organization Name and Address University of Florida 1949 Stadium Rd. Room 365 P.O. Box 116580 Gainesville, FL 32611		10. Work Unit No. (TRAIS)	
		11. Contract or Grant No. BDV31 TWO 977-102	
12. Sponsoring Agency Name and Address Florida Department of Transportation 605 Suwannee Street, MS 30 Tallahassee, FL 32399		13. Type of Report and Date	
		14. Sponsoring Agency Code	
15. Supplementary Notes			
16. Abstract This Phase 2 report continues research investigating the effects that installation and removal of sheet pile walls (SPWs) have on driven piles founded in granular soils. The method of analysis employed in Task 5 of Phase 1 of this project are extended to model systems involving a driven pile in proximity to two SPWs forming the corner of a closed rectangular cofferdam. Numerical simulations are presented which employ a combined Finite Element Method-Discrete Element Method (FEM-DEM) procedure which explicitly capture the mechanical behavior of the pile-soil-SPW system. Three relevant physical scenarios are studied, with a top-down load test following: (1) Pile driving into sand; (2) SPWs installation one at a time followed by pile driving into sand; and, (3) SPW installation, pile driving, and subsequent SPW removal one at a time in reverse sequence. The Davisson and ultimate capacities of the driven pile are therefore assessed in the presence of a driven SPW cofferdam, as well as in a soil from which the SPW structure has been recently removed. The response of the pile is shown to be dependent on geometrical parameters of the system; a parametric study is therefore performed with respect to the ratio of SPW cofferdam embedment depth versus the embedment depth of the pile. The components of total resistance are studied with respect to the pile's tip resistance and side friction; the relationships of these components to the presence or removal of the SPWs at various embedment depths are recorded. The results are condensed into a series of simple design charts which quantify the effects of the SPW cofferdam in scenarios 2 and 3 on the bearing capacities of the pile. Recommendations for the use of these graphical tools are presented for the easy quantification of these influences for the engineer facing relevant design decisions.			
17. Key Words Bearing capacity; Dislocation (Geology); Pile driving; Resistance (Mechanics); Sheet pile walls; Soil mechanics		18. Distribution Statement No restrictions.	
19. Security Classif. (of this report) Unclassified	20. Security Classif. (of this page) Unclassified	21. No. of Pages	22. Price

ACKNOWLEDGEMENTS

The authors would like to thank the Florida Department of Transportation (FDOT) for providing the funding that made this project possible.

EXECUTIVE SUMMARY

On the basis of the obtained numerical and physical test results, disturbance in a compacted soil condition caused by the removal of pre-installed sheet pile walls (SPW) may result in substantial loss in the end bearing of pile foundations. Deep SPW installation followed by extraction after pile installation requires considerable reduction of Davisson capacity that could undermine the superstructure support and cause excessive displacement. A combined Finite Element Method-Discrete Element Method (FEM-DEM) numerical procedure is extended to predict and quantify this phenomena when a pile is driven in the vicinity of two SPWs forming the corner of an enclosed rectangular cofferdam.

TABLE OF CONTENTS

DISCLAIMER	i
SI (MODERN METRIC) CONVERSION FACTORS (from FHWA).....	ii
ACKNOWLEDGEMENTS.....	v
EXECUTIVE SUMMARY	vi
LIST OF FIGURES	ix
LIST OF TABLES.....	xi
1. INTRODUCTION	1
1.1 Project Overview	1
1.2 Description of Numerical Models.....	1
1.2.1 Overview.....	1
1.2.2 Model Components and Simulation Sequence	1
1.2.3 Representative Model for Parametric Study	3
2. PARAMETRIC STUDY OF PILE-SOIL-SHEET PILE WALL COFFERDAM SYSTEMS ...	4
2.1 Considerations for Parameter Selection.....	4
2.1.1 Overview.....	4
2.1.2 Relative Embedment Depth.....	4
2.2 Simulation Matrix	4
2.3 Parametric Study Results	5
2.3.1 Overview.....	6
2.3.2 Top-Down Load-Displacement Behaviors when Controlling for Relative Embedment Depth for variation of ratio of embedment depth of cofferdam tip to the depth of tip of pile.....	6
3. RECOMMENDATIONS FOR PILE DESIGN	16
3.1 Overview.....	16
3.2 Accounting for Relative Embedment Depth.....	16
3.3 Recommended Use of Graphical Design Tools.....	24
4. SUMMARY AND CONCLUSIONS	26
4.1 Summary Regarding Work Completed Toward Phase 2.....	26
4.2 Conclusions.....	26

5. REFERENCES28

LIST OF FIGURES

<u>Figure</u>	<u>Page</u>
Figure 1.1 Schematic of scenario 1 test setup.....	2
Figure 1.2 Schematic for scenario 2 and scenario 3 setup.....	3
Figure 2.1 Total pile resistance for loading scenario 2 with horizontal distance between pile and SPWs equal to 4 ft.....	7
Figure 2.2 Skin friction component of total pile resistance for loading scenario 2 with horizontal distance between pile and SPWs equal to 4 ft	7
Figure 2.3 End bearing component of total pile resistance for loading scenario 2 with horizontal distance between pile and SPWs equal to 4 ft	8
Figure 2.4 Total pile resistance for loading scenario 3 with horizontal distance between pile and SPWs equal to 4 ft.....	9
Figure 2.5 Skin friction component of total pile resistance for loading scenario 3 with horizontal offset distance between pile and SPWs equal to 4 ft	10
Figure 2.6 End bearing component of total pile resistance for loading scenario 3 with horizontal offset distance between pile and SPWs equal to 4 ft	11
Figure 2.7 Location of stress sampling in the vicinity of pile tip for loading scenario 3	12
Figure 2.8 Locations within granular assembly between pile and SPWs from where horizontal stresses are sampled for loading scenario 3: (a) aerial view; (b) Section AA'	13
Figure 2.9 Horizontal stresses (YY) sampled between SPW1 and pile (location 1 in Fig. 2.8a) plotted through the depth of granular assembly.....	14
Figure 2.10 Horizontal stresses (XX) sampled between SPW2 and pile (location 2 in Fig. 2.8a) plotted through the depth of granular assembly.....	15
Figure 3.1 Change in total pile resistance at Davisson capacity for loading scenario 2 for different ratios of SPW embedment depth to pile embedment length	16
Figure 3.2 Change in total pile resistance at ultimate capacity for loading scenario 2 for different ratios of SPW embedment depth to pile embedment length.....	17
Figure 3.3 Change in total pile resistance at Davisson capacity for loading scenario 3 for different ratios of SPW embedment depth to pile embedment length	17

Figure 3.4 Change in total pile resistance at ultimate capacity for loading scenario 3 for different ratios of SPW embedment depth to pile embedment length.....	18
Figure 3.5 Change in skin friction component of total pile resistance at Davisson capacity for loading scenario 2 for different ratios of SPW embedment depth to pile embedment length	19
Figure 3.6 Change in skin friction component of total pile resistance at ultimate capacity for loading scenario 2 for different ratios of SPW embedment depth to pile embedment length	19
Figure 3.7 Change in skin friction component of total pile resistance at Davisson capacity for loading scenario 3 for different ratios of SPW embedment depth to pile embedment length	20
Figure 3.8 Change in skin friction component of total pile resistance at ultimate capacity for loading scenario 3 for different ratios of SPW embedment depth to pile embedment length	20
Figure 3.9 Change in end bearing component of total pile resistance at Davisson capacity for loading scenario 2 for different ratios of SPW embedment depth to pile embedment length	21
Figure 3.10 Change in end bearing component of total pile resistance at ultimate capacity for loading scenario 2 for different ratios of SPW embedment depth to pile embedment length	22
Figure 3.11 Change in end bearing component of total pile resistance at Davisson capacity for loading scenario 3 for different ratios of SPW embedment depth to pile embedment length	22
Figure 3.12 Change in end bearing component of total pile resistance at ultimate capacity for loading scenario 3 for different ratios of SPW embedment depth to pile embedment length	23

LIST OF TABLES

<u>Tables</u>	<u>Page</u>
Table 2.1 Test matrix of parametric study for loading scenarios 2 and 3.....	5
Table 2.2 Volume averaged stresses within granular assembly in the vicinity of pile the vicinity of pile tip for loading scenarios 1 and 2.....	11
Table 2.3 Volume-averaged stresses within granular assembly in the vicinity of pile the vicinity of pile tip for loading scenario 3	12
Table 3.1 Change in Davisson and ultimate capacity with respect to scenario 1, in terms of total force.	18
Table 3.2 Change in Davisson and ultimate capacity with respect to scenario 1, in terms of skin friction force.....	21
Table 3.3 Change in Davisson and ultimate capacity with respect to scenario 1, in terms of end bearing force.	23

CHAPTER 1

INTRODUCTION

1.1 Project Overview

In Phase 1 of the current project, a methodology was developed for the assessment of the influence of the proximity of sheet pile walls (SPWs) on the load capacity of piles driven into granular materials. This methodology combined a series of empirical centrifuge tests with a combined finite element method and discrete element method (FEM-DEM) numerical model. The results of the empirical and numerical analyses showed good agreement, and recommendations for pile design were prescribed in reference to the geometric configuration of the soil-pile-SPW system. The goal of the present study is to extend the numerical modelling methodology to cases involving the installation and removal of two SPWs forming a corner of an enclosed, rectangular cofferdam.

1.2 Description of Numerical Models

Numerical models were developed in order to simulate three distinct testing scenarios as a part of Phase 1 of this project. The combined finite element method and discrete element method (FEM-DEM) numerical model that was created to represent the geo-structural system corresponding a driven pile in proximity of an SPW is extended to represent a system corresponding a driven pile in the proximity of a corner of a rectangular cofferdam.

1.2.1 Overview

In this part of the report, a brief account of the different components of numerical model are discussed. For more technical details regarding the numerical procedure, see the Task 3.2 report of Phase 1 (Chung et al 2018b).

1.2.2 Model Components and Simulation Sequence

There are three major components of the numerical model used to simulate the loading scenarios of the geo-structural system: a granular assembly consisting of DSEs, structural elements like the pile and sheet pile walls consisting of shell elements, and the boundary consisting of a complex system of DSEs, springs and dampers. The complex boundary model was developed in order to impose local non-reflecting phenomenon on the particle elements in close proximity with the boundary. This is required to effectively create a semi-infinite domain using only a limited volume of elements. A more detailed account of the boundary condition modeling is given in the Phase 1 Task 3.2 report (Chung et al. 2018b).

The results of a model containing only a granular assembly, finite element pile, and the non-reflecting boundary conditions are taken from the Task 5 report of Phase 1 (Chung et a. 2018c). This numerical configuration will be referred to as scenario 1 in the present report, and is used as a benchmark for the influence of the SPW cofferdam. A schematic of the numerical model for scenario 1 is given in Fig. 1.1.

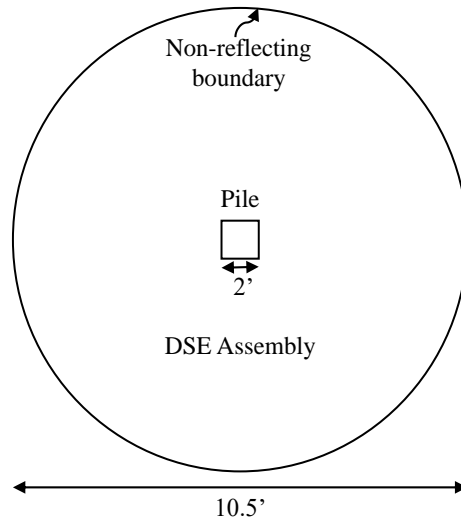


Figure 1.1 Schematic of scenario 1 test setup

Most of the components of the numerical model to simulate scenarios 2 and 3 are the same as those used for loading scenario 1 simulations. The new addition to the previous test setup is the SPW cofferdam. To accommodate SPW driving in the granular assembly at a prescribed distance from the pile and the boundary, a much larger granular assembly is required as compared to scenario 1 (where only the pile was introduced into the DSE assembly). This exponentially increases the number of elements required to mesh the entire volume for conducting system-scale simulations. Owing to the computational cost associated with running discrete element models, it becomes unfeasible to use such a small discrete element (as used in scenario 1) to mesh such a large volume. Hence, based on the dimension requirements for scenarios 2 and 3, a scaling factor was determined and the granular mesh used for scenario 1 was scaled up by that factor to create the larger domain while maintaining feasibility of practical simulation runtimes. A schematic for the scenarios 2 and 3 setup is given below (Fig. 1.2).

Scenarios 2 and 3 will include the installation of two SPWs, forming the corner of a rectangular cofferdam in the proximity of the driven pile. Prior to driving a pile model into the DSE assembly, representative SPW models, consisting of finite elements, are installed to simulate a corner configuration of square-shape cofferdam. The two independent finite element SPW models are driven one at a time to embedment depth ratios of 0.25 (4.5 ft), 0.5 (9 ft), 0.75 (13.5 ft) and 1.0 (18 ft) with respect to the pile embedment length of 18 ft (i.e., 9 times the pile width).

Scenarios 2 and 3 differ from one another with respect to the removal of SPWs. In scenario 2, the pile is subsequently driven at an offset distance of 4 ft (2 times the width of the pile). Once the pile reaches a target depth, prescribed vertical loading is applied and the predictions of load-settlement behavior are obtained. In scenario 3, the SPWs and pile are installed identically to scenario 2. However, after the pile installation, the two SPWs are then removed from the DSE assembly one at a time (SPW 2 is first completely removed, followed by SPW 1). A period of approximate 0.8 seconds (simulation time) is allowed for the dynamic effects of removal of SPWs to dissipate and for the assembly to reach its new equilibrium state. The prescribed vertical loading

is then applied after the removal of the SPWs, and the load-settlement behavior is assessed in the absence of the SPW cofferdam.

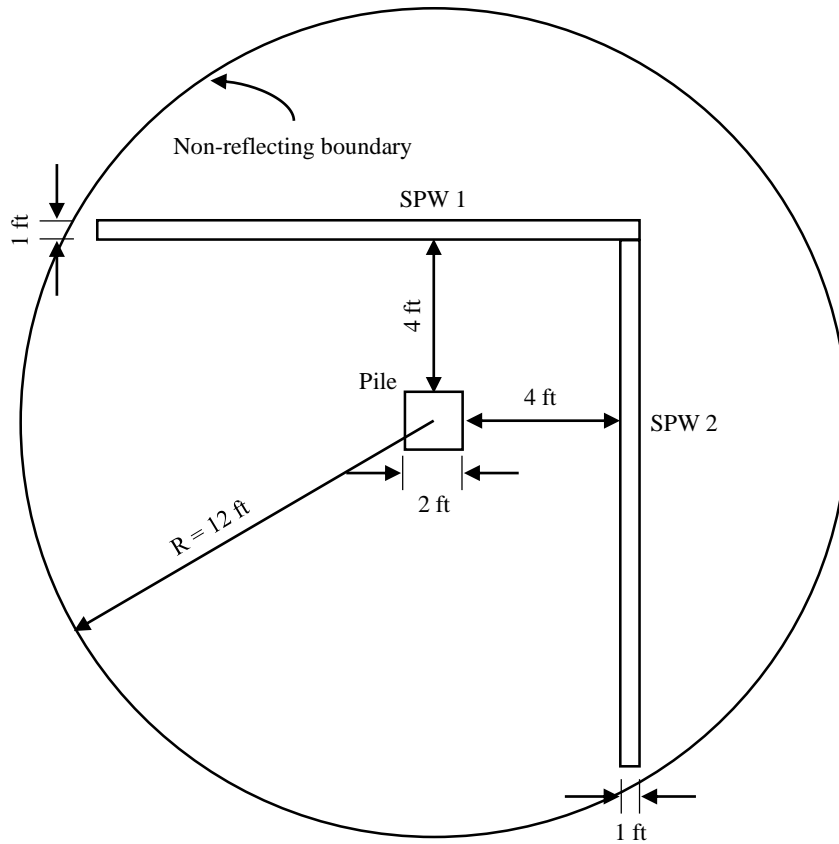


Figure 1.2 Schematic for scenario 2 and scenario 3 setup

1.2.3 Representative Model for parametric study

The benchmarked numerical model that was used to conduct the parametric sensitivity study as Task 5 of Phase 1 of this project will be used for current investigations. Detailed numerical simulation results and the benchmarking process can be found in Task 3.2 report (Chung et al. 2018b). Similar to Task 5 of Phase 1 (Chung et al. 2018c), the effects of the SPW cofferdam installation and removal in the pile capacities would be investigated using both simulation 6 and simulation 7 models per each of the geometric variations, i.e., SPW cofferdam installation distance and depth with respect to the pile location. However, the pile capacities from numerical simulations will be presented as an average between the pile capacities predicted by simulation 6 and simulation 7 for all the cases of geometric variations.

CHAPTER 2

PARAMETRIC STUDY OF PILE-SOIL-SHEET PILE WALL COFFERDAM SYSTEMS

2.1 Considerations for Parameter Selection

In the current phase of research, complex geo-structural systems consisting of the granular media, pile and sheet-pile wall in cofferdam configuration are closely investigated to identify and isolate the effects of relative embedment depth of SPW cofferdam corresponding to the depth of the pile tip at a fixed horizontal offset distance. This investigation is performed across both loading scenarios 2 and 3. Based on the simulation results, design recommendations are made to be used in order to obtain an approximate estimate of pile load capacity corresponding to various relative embedment depths of the cofferdam with respect to depth of pile tip.

2.1.1 Overview

In this part of the report, an account of selected geometric configuration parameters for parametric sensitivity study and their corresponding simulation results are discussed.

2.1.2 Relative Embedment Depth

The geometric parameter that is being investigated is the embedment depth of SPW cofferdam tip relative to the embedment depth of pile tip. The zone of influence in which the stress state within granular assembly is altered is affected by the depth up to which the cofferdam tip is embedded. The more the embedment depth, the larger this zone of influence is. The embedment depth of SPW tip is normalized with respect to the embedment depth of pile tip.

Pile tip is embedded to a depth of approximately 17.7 ft. For the current investigation, four different embedment depths for SPW tip are selected for investigation: 4.425 ft ($\frac{1}{4}$ Embedment depth); 8.85 ft ($\frac{1}{2}$ Embedment depth); 13.275 ft ($\frac{3}{4}$ Embedment depth); and 17.7 ft (full Embedment depth). The pile is driven at a horizontal offset distance of 4 ft (two times the width of pile) from the face of both the SPWs constituting the cofferdam configuration (see Fig. 1.2).

2.2 Simulation Matrix

Based on the above identified parameters, a test matrix for all the simulations that were performed as the part of the investigation is created. Parametric study is carried out using both the simulation 6 and simulation 7 numerical models from Task 3 of Phase 1. However, the results in the subsequent sections have been calculated as an average value between the two. The test matrix for all the simulations as a part of parametric study is given below (Table 2.1).

Table 2.1 Test matrix of parametric study for loading scenarios 2 and 3

Simulation	Horizontal offset distance between pile and faces of two SPWs constituting the cofferdam (ft)	Ratio of cofferdam embedment depth to pile tip depth
6	4	$\frac{1}{4}$
	4	$\frac{1}{2}$
	4	$\frac{3}{4}$
	4	1
7	4	$\frac{1}{4}$
	4	$\frac{1}{2}$
	4	$\frac{3}{4}$
	4	1

Simulation results from the parametric study are discussed in the following sections.

2.3 Parametric Study Results

Numerical simulations are carried as per the test matrix defined in the previous section. Quasi-static top-down load-displacement behavior is the main focus of this report as the objective of this report is to provide design recommendations.

2.3.1 Overview

In this part of the report, the Davisson and ultimate load capacities of the driven pile are presented for scenario 2 and scenario 3, which are average values obtained from the lower (simulation 6) and upper (simulation 7) bound solutions.

2.3.2 Top-Down Load-Displacement Behaviors for variation of ratio of embedment depth of cofferdam tip to the depth of tip of pile

The quasi-static top-down load-displacement behavior of the SPW-pile system is investigated for geometric parameters of relative depths between pile tip and SPW toe. Results of pile resistance are shown in Fig. 2.1-2.3 under scenario 2 loading conditions. Fig. 2.1 show the force-displacement plots with respect to the total force on the pile. A pattern emerges with respect to relative depth of cofferdam toe corresponding to the depth of pile tip; the deeper cofferdam is pre-installed the greater maximum load carrying capacity. For example, the axial resistance predicted at relative depth ratio of 1.0 is much greater than that at relative depth ratio of 0.25. The lateral confinement substantially increases as movement of granular mass is constrained to an extent by the proximity of SPWs.

Fig. 2.2 show the force-displacement behavior with respect to the components of the side skin friction. As the ratio of embedment depth increases, the effects of additional lateral resistance can be seen in the drastic increase in side friction, with over 100% increase in side frictional force at full embedment ratio. The presence of structural element in the vicinity of the pile resists lateral movement of granular mass, resulting in larger magnitudes of horizontal confinement on the pile. The confinement of the granular packing increases the resulting frictional forces between individual grains and the driven pile, leading to a significant increase in the resistance of the granular mass to penetration.

The presence of the SPWs also lead to a similar but not as pronounced increase in the component of end-bearing resistance, as shown in Fig. 2.3. The pattern in increased total bearing resistance is therefore brought on by both increased skin friction and end bearing capacity. This suggests that the presence of SPWs effects the granular packing in such a way that it increase both its lateral and vertical resistance. The confining effect of the SPWs on the granular mass leads to a new, more densely packed initial state in which the inter-particle friction is increased. Thus, the end bearing component of resistive force also increases as the SPWs are driven to larger relative depths.

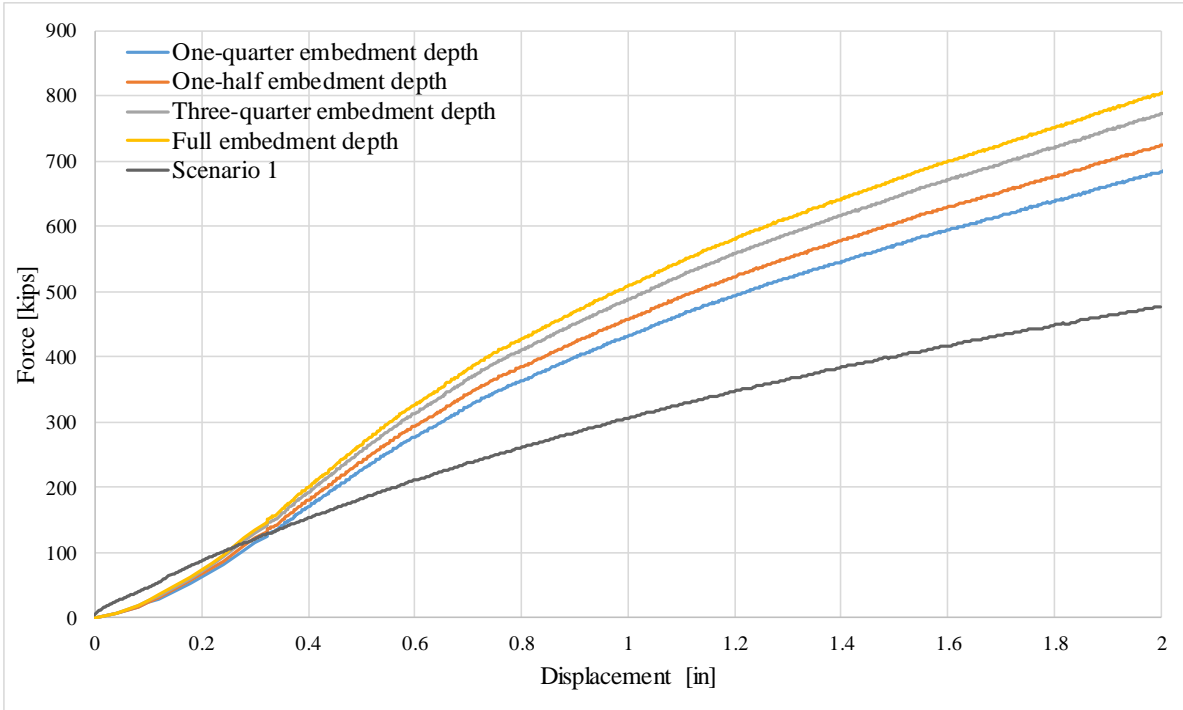


Figure 2.1 Total pile resistance for loading scenario 2 with horizontal distance between pile and SPWs equal to 4 ft

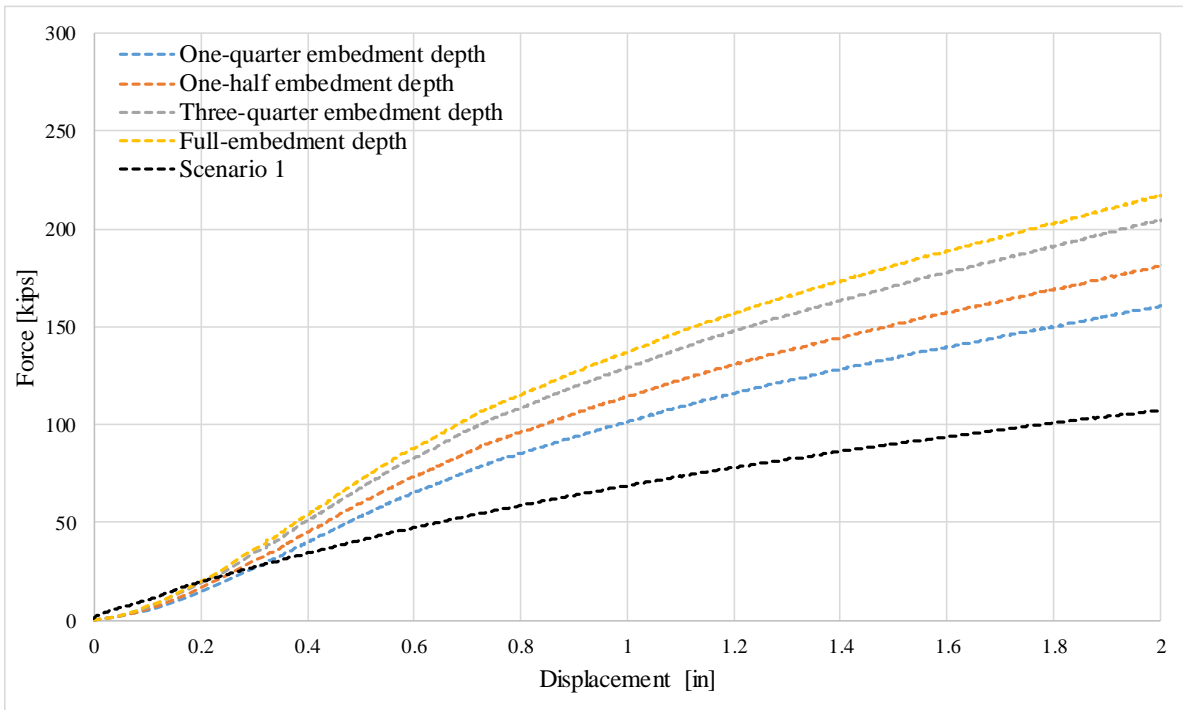


Figure 2.2 Skin friction component of total pile resistance for loading scenario 2 with horizontal distance between pile and SPWs equal to 4 ft

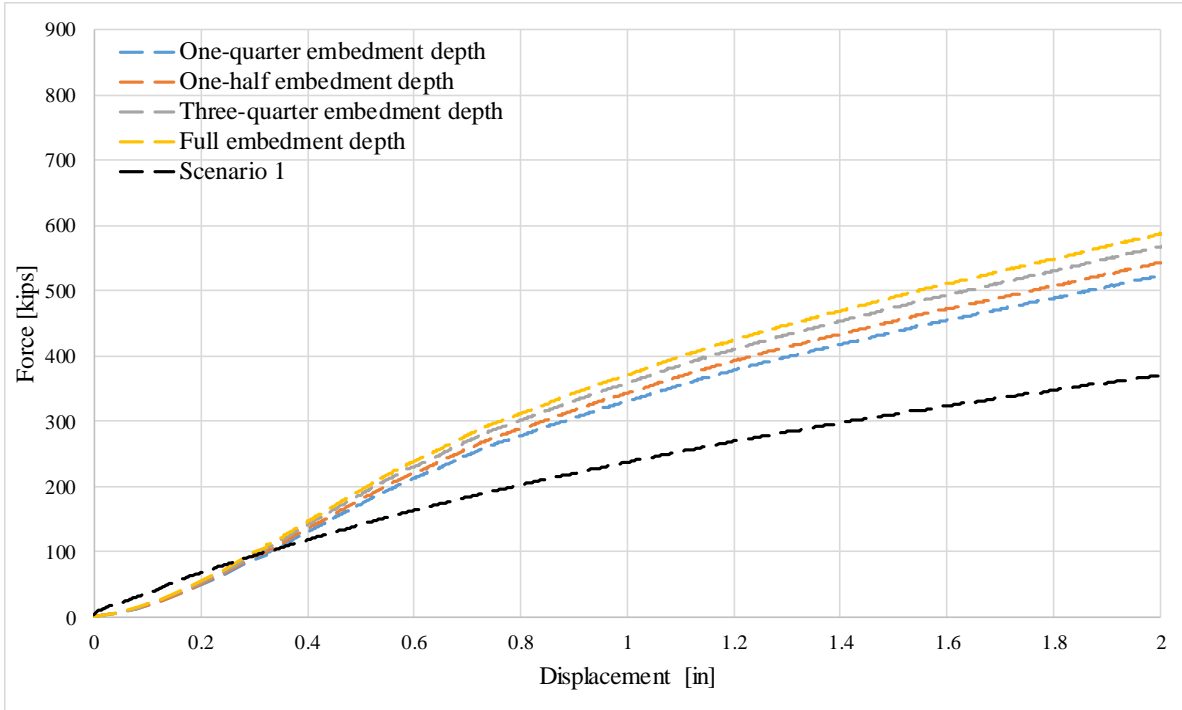


Figure 2.3 End bearing component of total pile resistance for loading scenario 2 with horizontal distance between pile and SPWs equal to 4 ft

In Fig. 2.4, the total pile resistance is plotted with displacement for loading scenario 3. A reverse trend of scenario 2 is observed for scenario 3 where reduction in the pile capacities is evident. Recall that the pile load capacity drastically increases in scenario 2 (Fig. 2.1) where we observe about a maximum of 72% difference in the ultimate capacity, depending on SPW embedment depths. On extraction of SPWs, a significant drop in the pile capacity is observed. A maximum drop of 25% for total pile resistance at ultimate pile capacity was estimated whereas, a maximum drop of 60% for total pile resistance at Davisson capacity was estimated. A more pronounced effect of SPW extraction on Davisson capacity can be attributed to the loosening of granular mass in the region between SPWs and pile. The highest effect of SPW extraction is seen for the case of highest relative depth ratio as the zone of influence is much larger than the other cases.

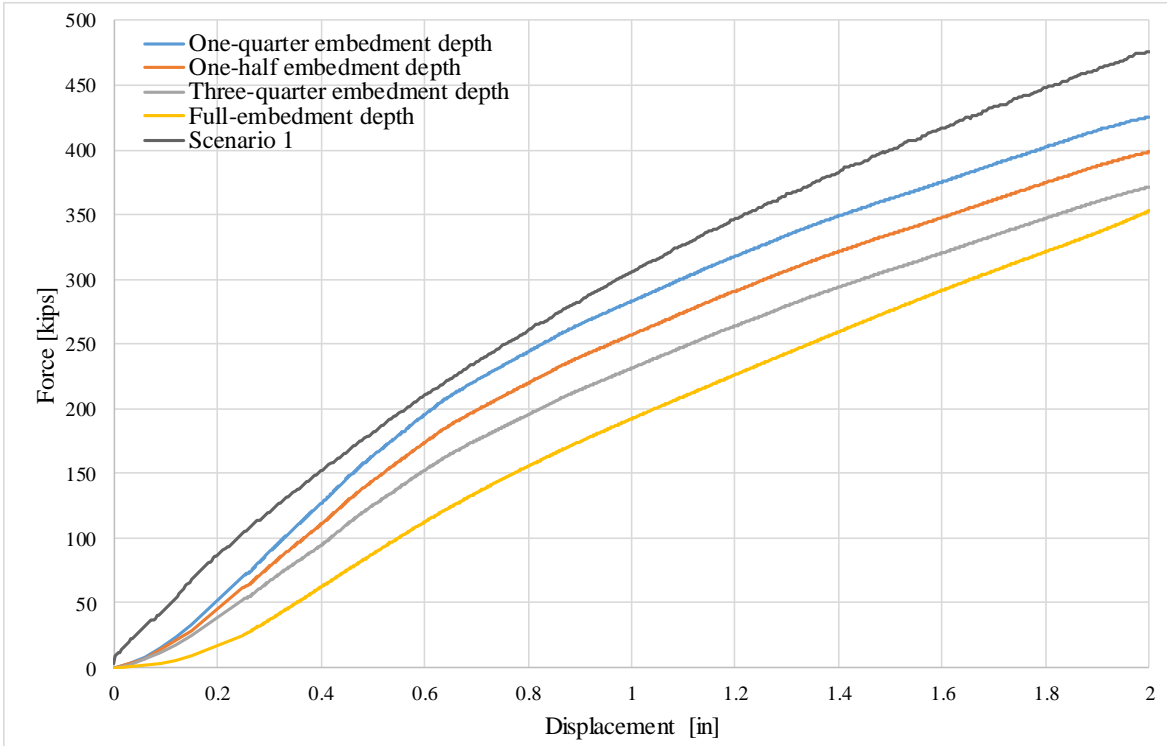


Figure 2.4 Total pile resistance for loading scenario 3 with horizontal distance between pile and SPWs equal to 4 ft

In Fig. 2.5, the skin friction component of pile resistance are plotted with displacement for loading scenario 3. It is evident from the force-displacement plots that the extraction of SPWs from the vicinity of the pile substantially reduces the skin friction component of total resistance. For the case of embedment depth equal to depth of pile tip, more than half of the skin friction is lost on removal of SPWs at Davisson capacity. On extraction, a void is created in the granular assembly in the space originally occupied by the SPWs. The geometrical arrangement between granules is disturbed and a state of unsteady equilibrium is reached. Granular rearrangement takes place within the assembly so as to achieve a steady state of equilibrium. Some of the void space is recovered by the granular rearrangement but there is a net loss in inter-particle jamming. This results in the reduction of lateral forces acting on the pile and subsequently reduces the frictional resistance acting on the side of the pile. This effect is more pronounced for higher embedment depths of SPW as the void space created on extraction of SPWs is much larger resulting in particle rearrangement in a larger volume of granular assembly.

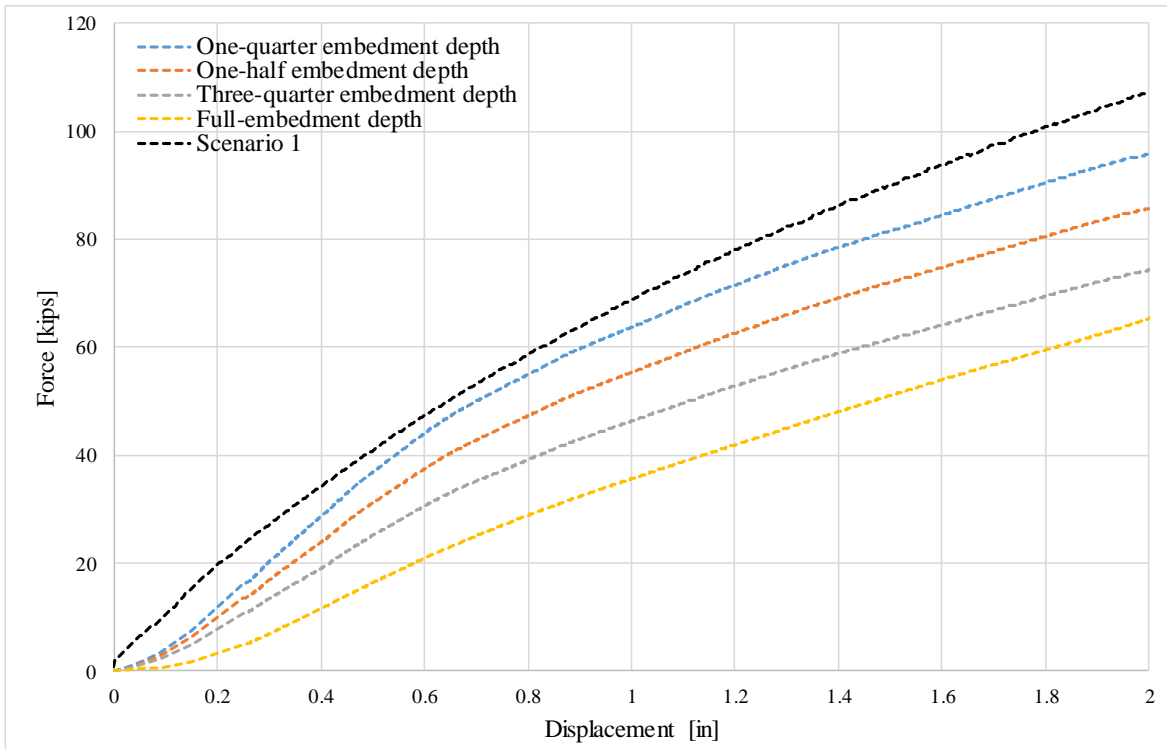


Figure 2.5 Skin friction component of total pile resistance for loading scenario 3 with horizontal offset distance between pile and SPWs equal to 4 ft

In Fig. 2.6, the end bearing component of total pile resistance are plotted with displacement of the pile for loading scenario 3. As was observed for the case of skin friction, the effect of extraction of SPWs on end bearing increases with increasing embedment depth of SPWs. At Davisson capacity, a maximum drop of about 60% is estimated for the case of SPW embedment depth equal to the pile driving depth. The effect of extraction of SPWs from the vicinity of the pile are still observed near the pile tip, however it is not as significant as for the case of skin friction. The presence of SPWs in the assembly alters the stress states of granular mass around the pile tip as well, as the pile tip is within the zone of influence. Subsequently, on the removal of SPWs, this stress state is further altered resulting in the loss of end bearing resistance of the pile.

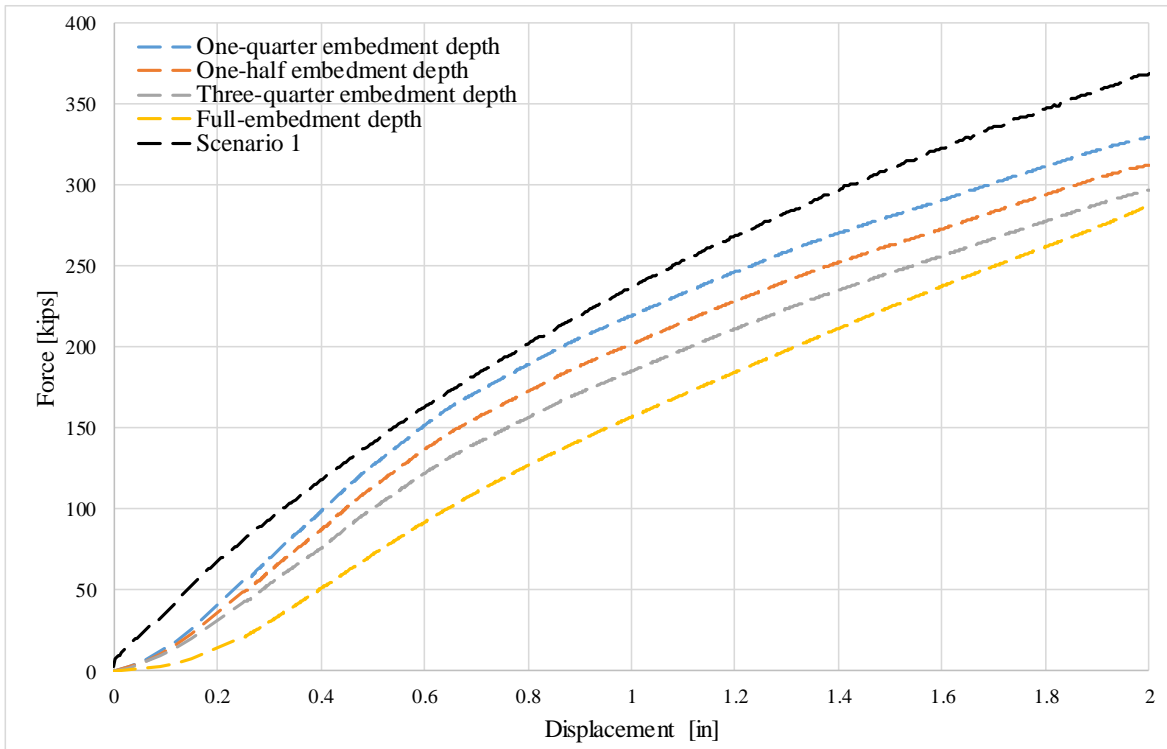


Figure 2.6 End bearing component of total pile resistance for loading scenario 3 with horizontal offset distance between pile and SPWs equal to 4 ft

To further study the phenomenon of reduction in pile capacity on removal of SPWs, stresses in the vicinity of the pile tip and stresses in the granular mass between SPWs and pile are calculated and plotted at different temporal states of loading scenario 3. We will look at the stresses in the vicinity of pile tip first. Volume-averaged vertical and horizontal stresses are estimated in the granular mass in the vicinity of the pile tip. The location of stress sampling is given in Fig. 2.7. Please note that the stresses computed below are for the case of embedment depth of SPWs equal to one-fourth of the depth of pile driving. The stresses are computed at four temporal states during loading scenario 3 – after completion of pile driving, after removal of first SPW, after removal of second SPW and finally just prior to the beginning of the top-down load test (Table 2.3). For comparison purposes, the stresses for loading scenarios 1 and 2 sampled from the same location in the granular assembly just prior to the beginning of top-down load test are computed (Table 2.2).

Table 2.2 Volume averaged stresses within granular assembly in the vicinity of pile the vicinity of pile tip for loading scenarios 1 and 2

Temporal states	Loading scenario	Simulation 6		Simulation 7	
		Horizontal stress (ksi)	Vertical stress (ksi)	Horizontal stress (ksi)	Vertical stress (ksi)
Just prior to beginning of top-down load test	Scenario 1	0.923	1.468	0.981	1.671
	Scenario 2	0.961	1.67	1.107	1.902

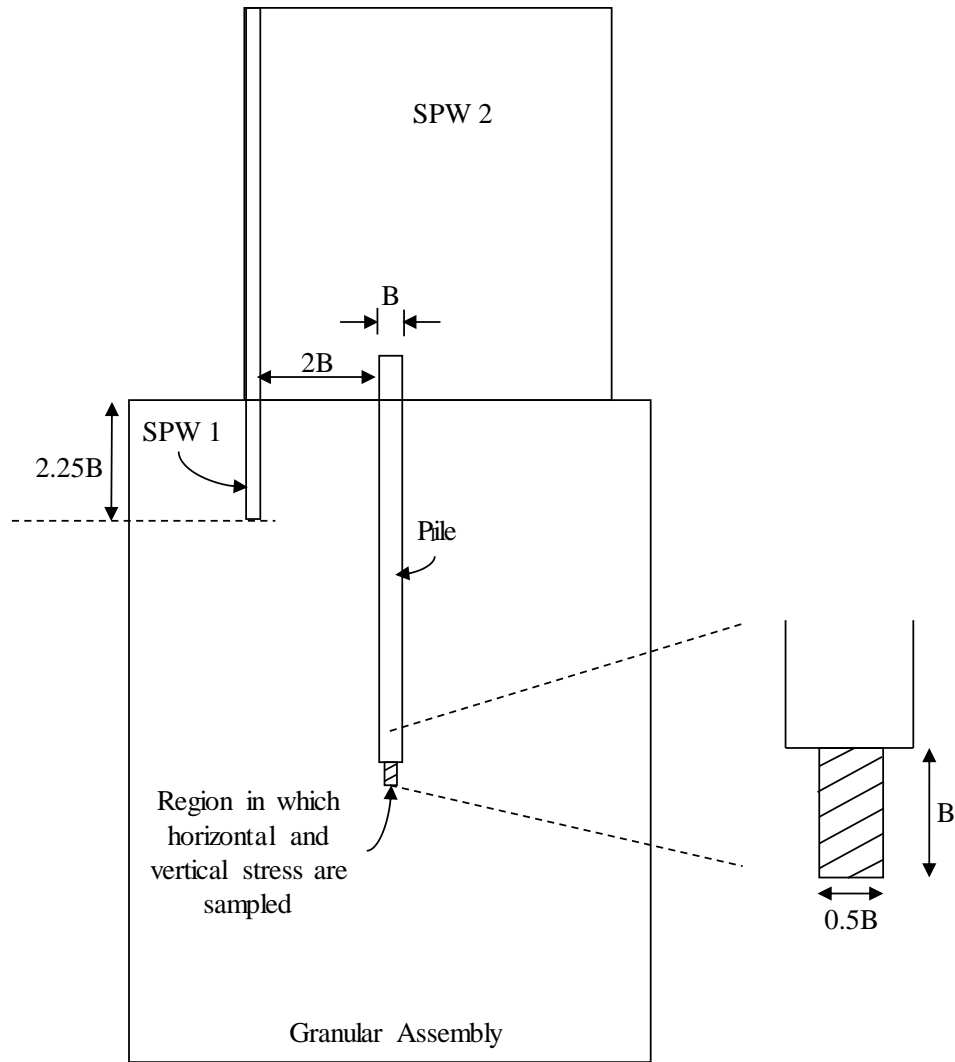


Figure 2.7 Location of stress sampling in the vicinity of pile tip for loading scenario 3

Table 2.3 Volume-averaged stresses within granular assembly in the vicinity of pile the vicinity of pile tip for loading scenario 3

Temporal states	Simulation 6		Simulation 7	
	Horizontal stress (ksi)	Vertical stress (ksi)	Horizontal stress (ksi)	Vertical stress (ksi)
After piling driving	0.961	1.67	1.107	1.902
After removal of first SPW	0.872	1.534	1.005	1.748
After removal of second SPW	0.843	1.503	0.972	1.712
Just prior to beginning of top down load test	0.8402	1.487	0.969	1.694

In Table 2.3, the effect of removal of SPWs is clearly indicated by the volume-averaged stresses at different temporal states during loading scenario 3. To understand the effect of SPWs on the top-down load test results for loading scenarios 2 and 3 (plotted in Figs. 2.1 through 2.6), the stress states prior to the beginning of top-down load tests are of interest. It can be concluded from Tables 2.2 and 2.3, that there is significant difference in the stresses in the vicinity of the pile for all the loading scenarios. Between loading scenarios 1 and 2, there is a significant increase in the stresses, while between scenarios 1 and 3, there is a significant reduction in the stress. It is pointed out that these stresses are calculated for the case of embedment depth ratio of 0.25. These effects will be much more pronounced for the cases of higher embedment ratios.

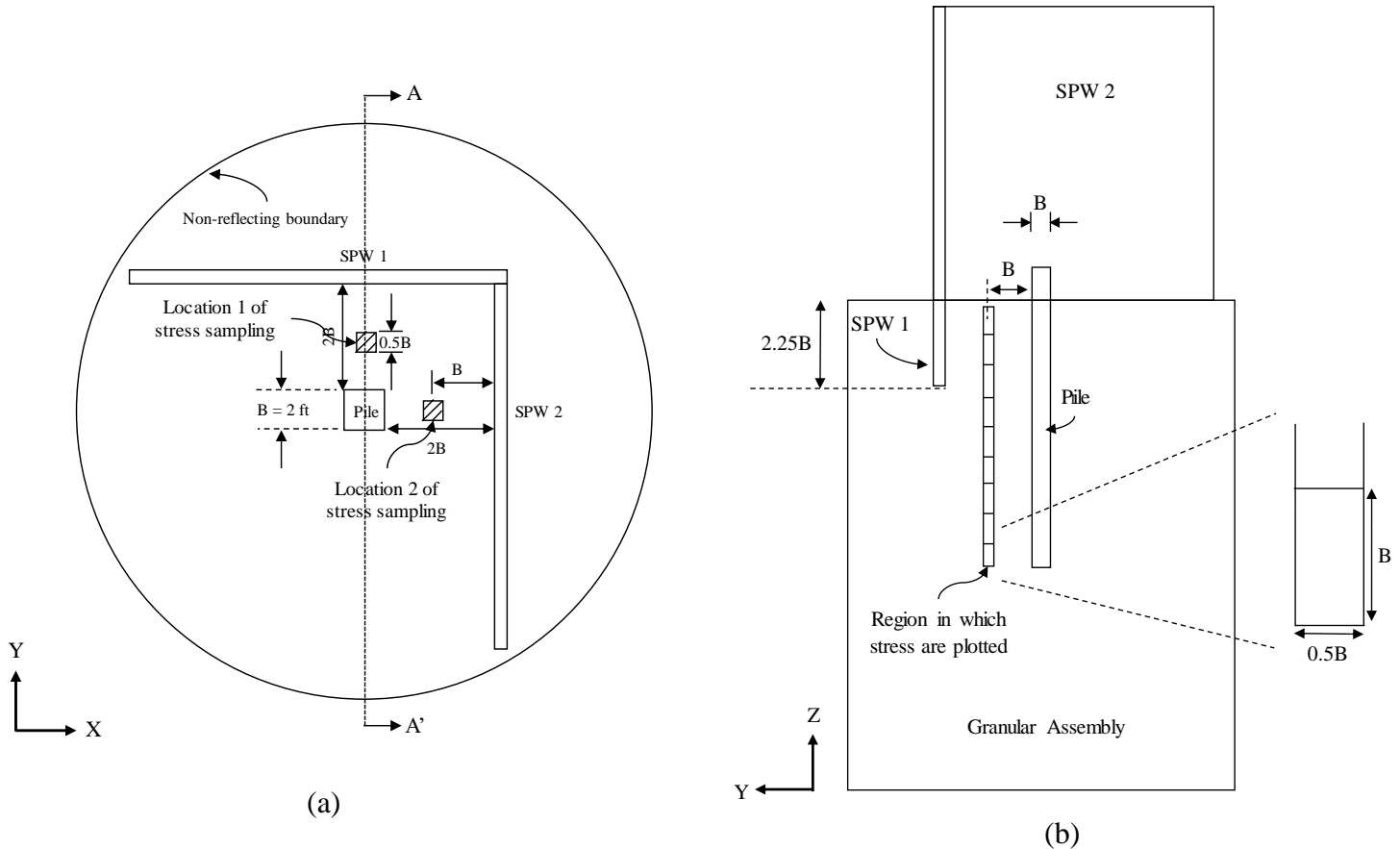


Figure 2.8 Locations within granular assembly between pile and SPWs from where horizontal stresses are sampled for loading scenario 3: (a) aerial view; (b) Section AA'

To understand the effects of SPWs on the lateral forces acting on the pile (skin friction component of total resistance), horizontal stresses are sampled from the regions annotated in Fig. 2.8, and volume-averaged over a selected control volume. As there are two SPWs present, the stresses are sampled between the pile and both the SPWs. The volume-averaged stresses are plotted as a function of depth of sampling from the granular assembly for four temporal states identical to the ones at which stresses in vicinity of pile are computed – after completion of pile driving, after removal of first SPW, after removal of second and just prior to the beginning of top-down load test.

In Figs. 2.9 and 2.10, the horizontal (YY) stresses sampled between SPW1 and the pile (location 1 in Fig. 2.8), and the horizontal (XX) stresses sampled between SPW2 and the pile are plotted with depth for loading scenario 3, respectively. To understand the effect of SPW on top-down load test results, the stress state just prior to the beginning of top-down load test are of interest. It must be noted that the stress state after completion of pile driving in Figs. 2.9 and 2.10 for loading scenario 3, also represent the stress state after completion of pile driving for loading scenario 2, as loading scenarios 2 and 3 are identical up to that stage. Also, of importance is to note that for loading scenario 2, the stress state after completion of pile driving will be almost identical to the stress state just prior to beginning of top-down load test. Therefore, this can be used for comparing the stress states just prior to beginning of top-down load test between loading scenarios 2 and 3.

From Fig. 2.9, it can be seen that as the SPWs are removed, there is progressive loss of horizontal (lateral) stresses in the granular assembly. This is also indicative of the loss of skin friction component of total pile resistance. A similar loss in lateral stresses is observed in Fig. 2.10. The combined effect of loss of lateral stresses in Figs. 2.9 and 2.10 result in the net loss of skin friction component of total pile resistance.

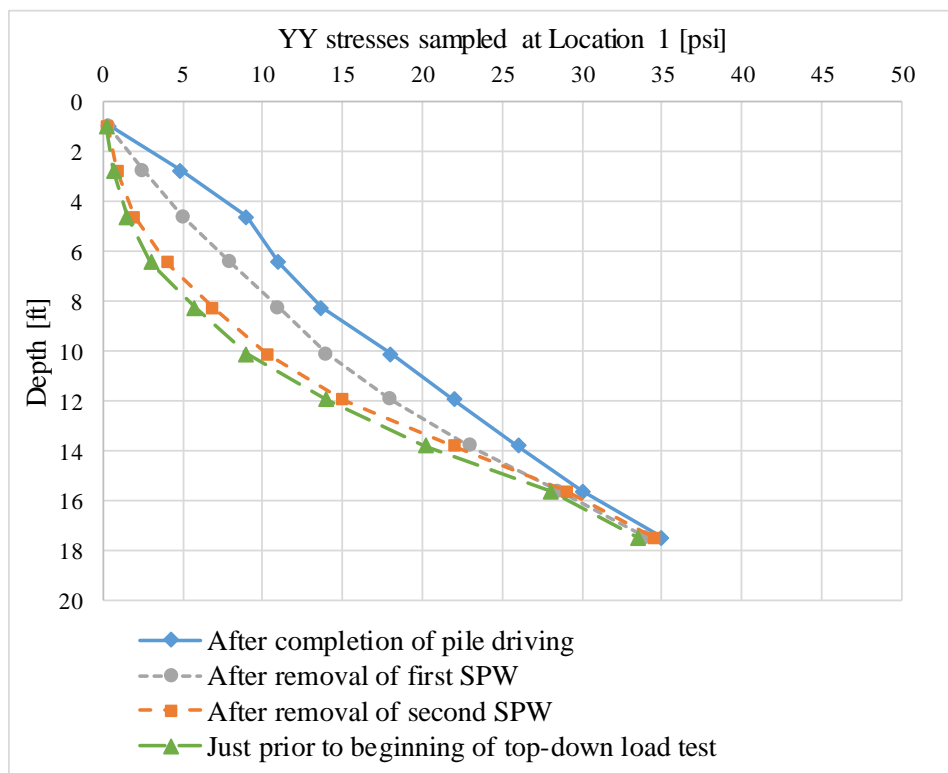


Figure 2.9 Horizontal stresses (YY) sampled between SPW1 and pile (location 1 in Fig. 2.8a) plotted through the depth of granular assembly

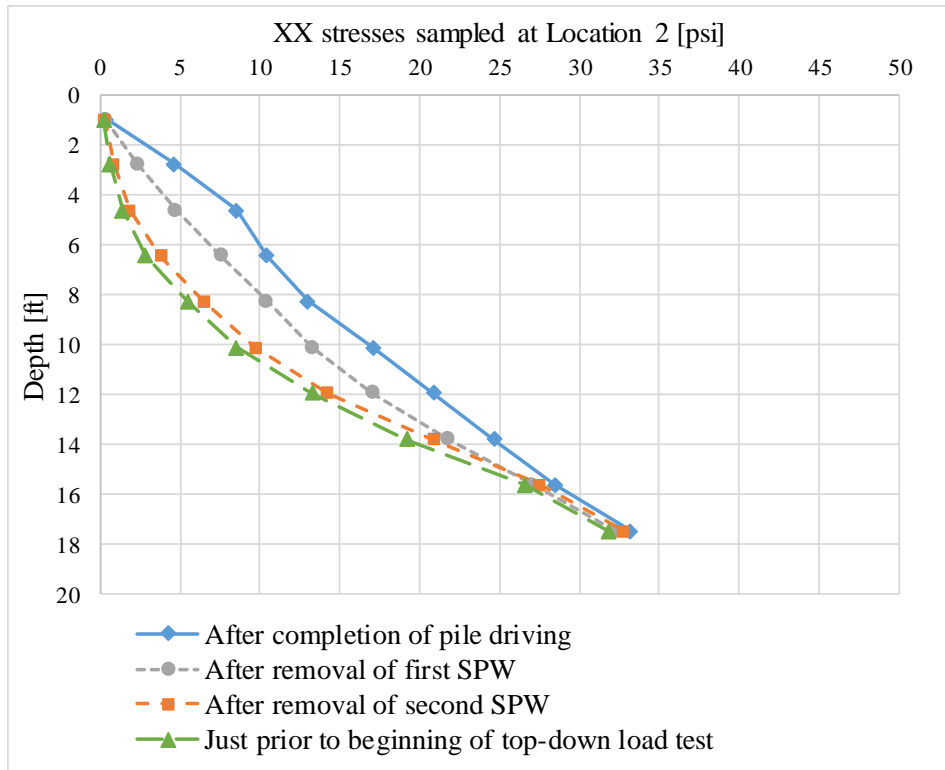


Figure 2.10 Horizontal stresses (XX) sampled between SPW2 and pile (location 2 in Fig. 2.8a) plotted through the depth of granular assembly

CHAPTER 3 RECOMMENDATIONS FOR PILE DESIGN

3.1 Overview

In this chapter, design considerations are presented with respect to the geometric parameters of the two SPWs-pile system. In particular, the predictions of pile capacities under loading scenario 2 and scenario 3 are made to account for the effect of the pre-installation and post removal of the SPWs in comparison to the single pile system of loading scenario 1; i.e., pile resistance estimated for loading scenarios 2 and 3 numerical simulations are presented in terms of percentage change with respect to the pile resistance estimated for the single pile system (loading scenario 1). In this way, engineers can estimate pile capacities using multipliers as factors of geometric configurations of the two SPW-pile foundation system both before and after extraction of SPWs if the pile capacity of a single pile system is known.

3.2 Accounting Relative Embedment Depth

As shown in Fig. 3.1 and Fig. 3.2, the increase in total pile resistance for loading scenario 2 are presented for different ratios of SPW embedment depth to pile embedment length. In relation to pile load capacity of the single pile foundation, Davisson and ultimate pile capacities for this scenario can be assessed in a straightforward manner for the percentage changes per incremental SPW pre-embedment depths. As can be seen from both the plots, the total pile resistance for loading scenario 2 relative to the pile resistance for single pile system increases with increase in the embedment depth ratio.

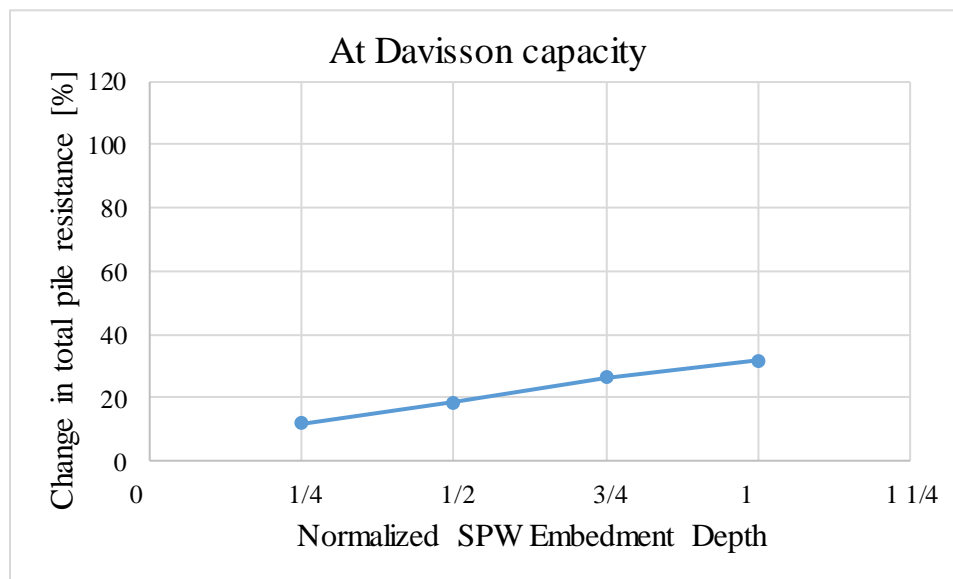


Figure 3.1 Change in total pile resistance at Davisson capacity for loading scenario 2 for different ratios of SPW embedment depth to pile embedment length

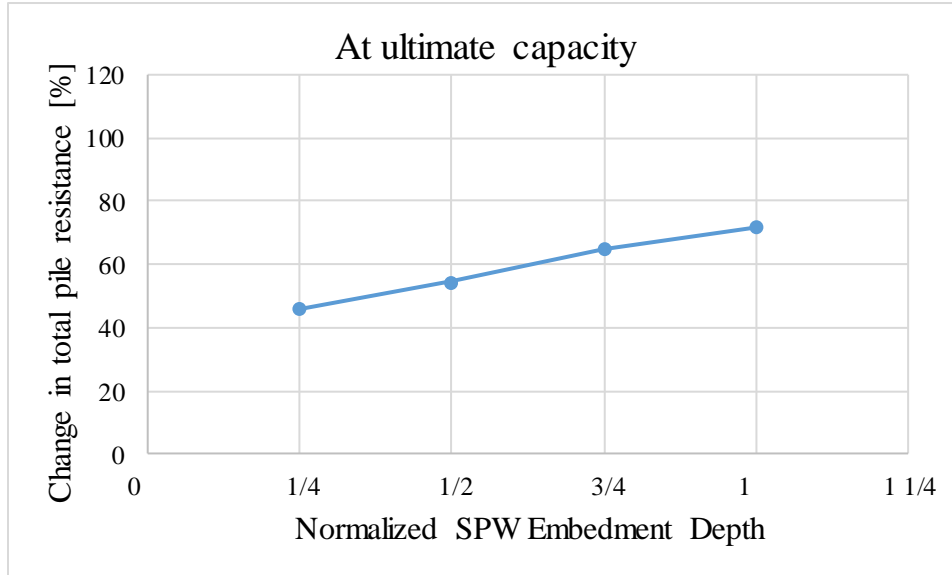


Figure 3.2 Change in total pile resistance at ultimate capacity for loading scenario 2 for different ratios of SPW embedment depth to pile embedment length

In contrast, the total pile resistance at Davisson and ultimate capacities decreases upon the removal of SPWs as shown in Fig. 3.3 and Fig. 3.4 respectively. This trend is mainly due to decrease in the confinement of the granular packing which ultimately reduces the frictional and normal resistive forces on the pile. The reduction relative to the pile capacities of scenario 1 can be interpreted as a function of the ratio of SPW embedment depth to pile embedment length, which are presented as a graphical tool to estimate the Davisson and ultimate pile capacities of the pile foundation system after the removal of SPWs.

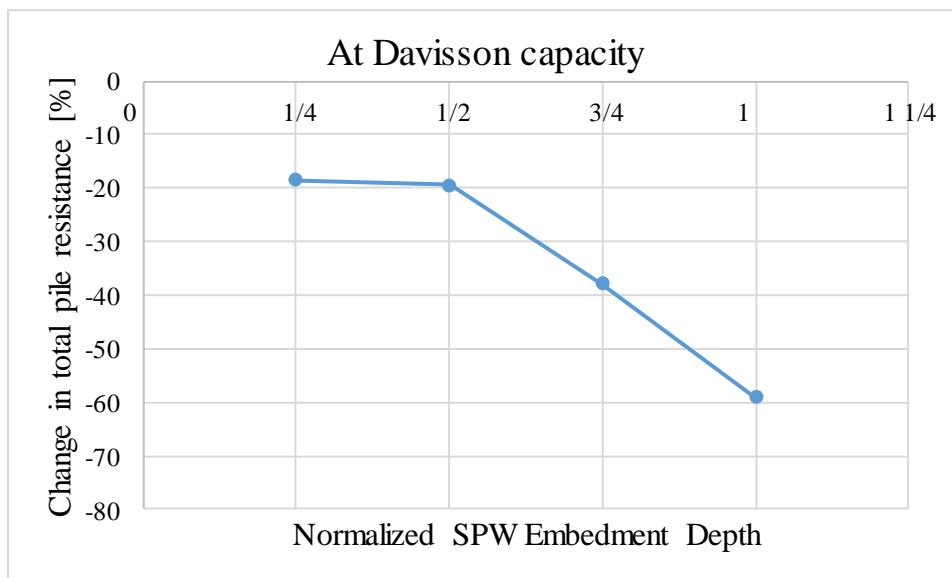


Figure 3.3 Change in total pile resistance at Davisson capacity for loading scenario 3 for different ratios of SPW embedment depth to pile embedment length

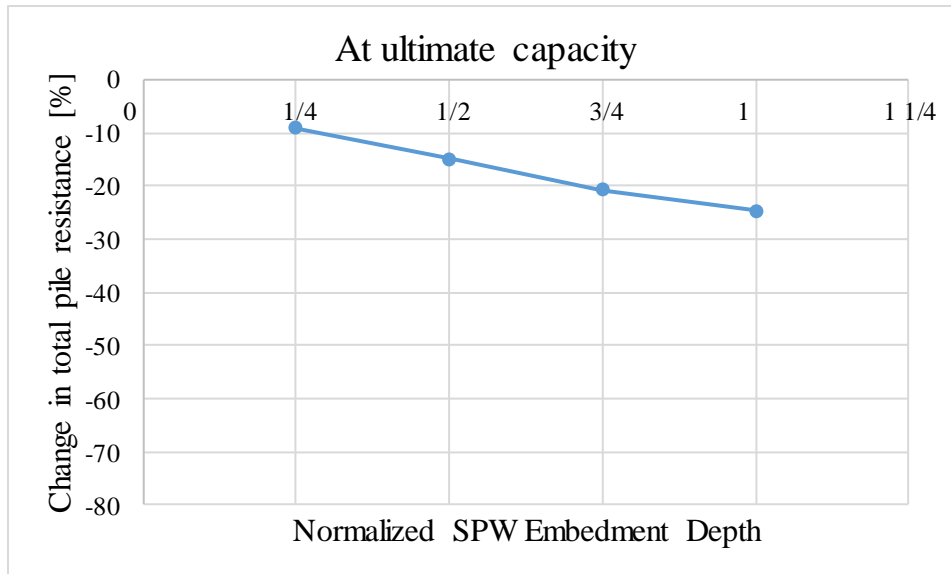


Figure 3.4 Change in total pile resistance at ultimate capacity for loading scenario 3 for different ratios of SPW embedment depth to pile embedment length

The percentage change in total pile resistance for loading scenarios 2 and 3 plotted in Figs. 3.1 through 3.4 are tabulated below (Table 3.1). The trend-lines from Figs. 3.1 through 3.4 and the percent change in table 3.1 can be used for estimating the total pile resistance of a two SPW-pile foundation system for any intermediate embedment depth ratio.

Table 3.1 Change in Davisson and ultimate capacity with respect to scenario 1, in terms of total force.

Scenario 1		Davisson capacity		Ultimate capacity	
		152.00		468.00	
	Embedment depth ratio	Scenario 2	Scenario 3	Scenario 2	Scenario 3
Capacity	one-quarter	170.07	123.95	683.50	425.58
	one-half	180.08	122.53	723.70	398.51
	three-quarter	192.08	94.60	771.95	371.43
	full	200.10	62.31	804.11	352.97
% change in capacity	one-quarter	11.89	-18.45	46.05	-9.06
	one-half	18.47	-19.39	54.64	-14.85
	three-quarter	26.37	-37.76	64.95	-20.63
	full	31.64	-59.01	71.82	-24.58

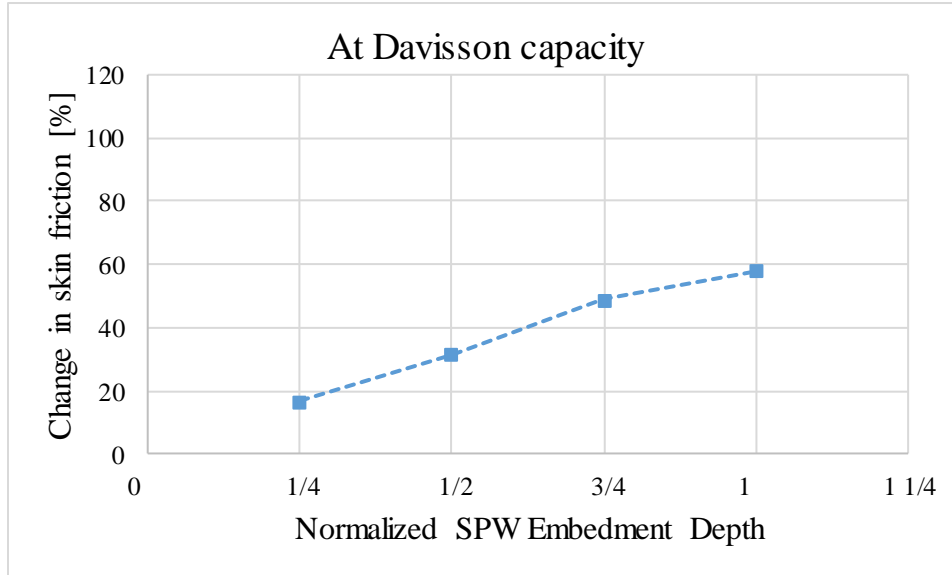


Figure 3.5 Change in skin friction component of total pile resistance at Davisson capacity for loading scenario 2 for different ratios of SPW embedment depth to pile embedment length

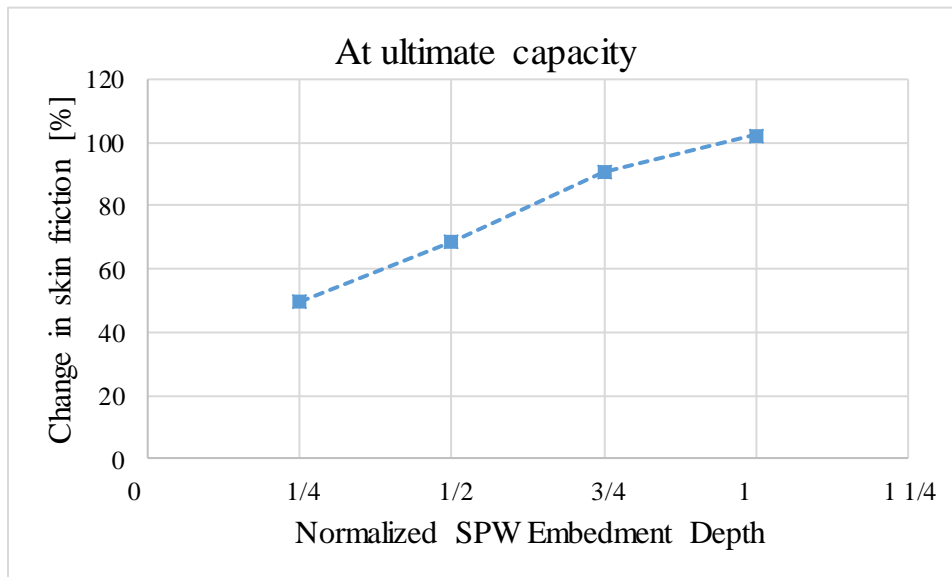


Figure 3.6 Change in skin friction component of total pile resistance at ultimate capacity for loading scenario 2 for different ratios of SPW embedment depth to pile embedment length

Figs. 3.5 and 3.6 show the increases in the skin friction component of total resistance which occur in scenario 2 for Davisson and ultimate capacities, respectively. These are given conveniently in terms of percentage of total skin friction. Figs. 3.7 and 3.8 show the corresponding reductions calculated for scenario 3. These values are listed in Table 3.2.

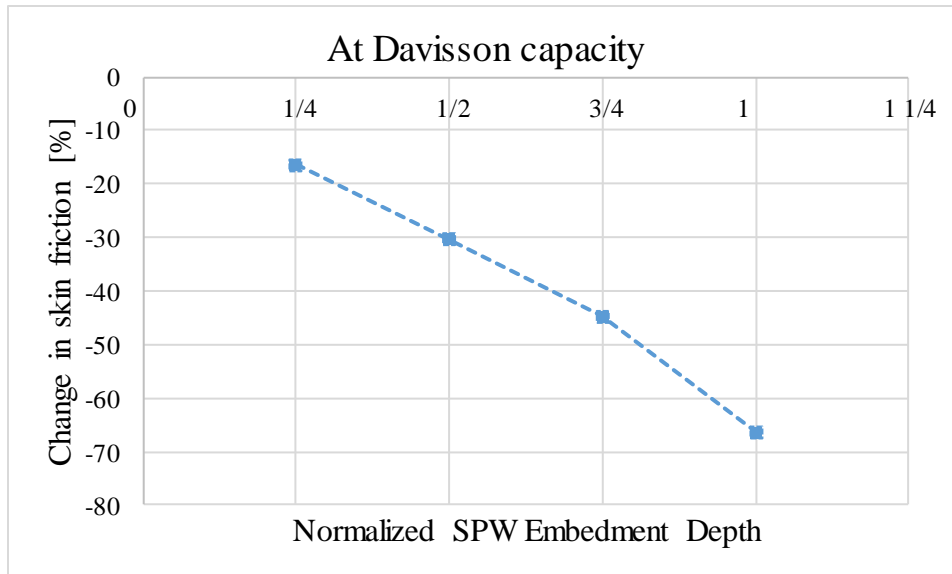


Figure 3.7 Change in skin friction component of total pile resistance at Davisson capacity for loading scenario 3 for different ratios of SPW embedment depth to pile embedment length

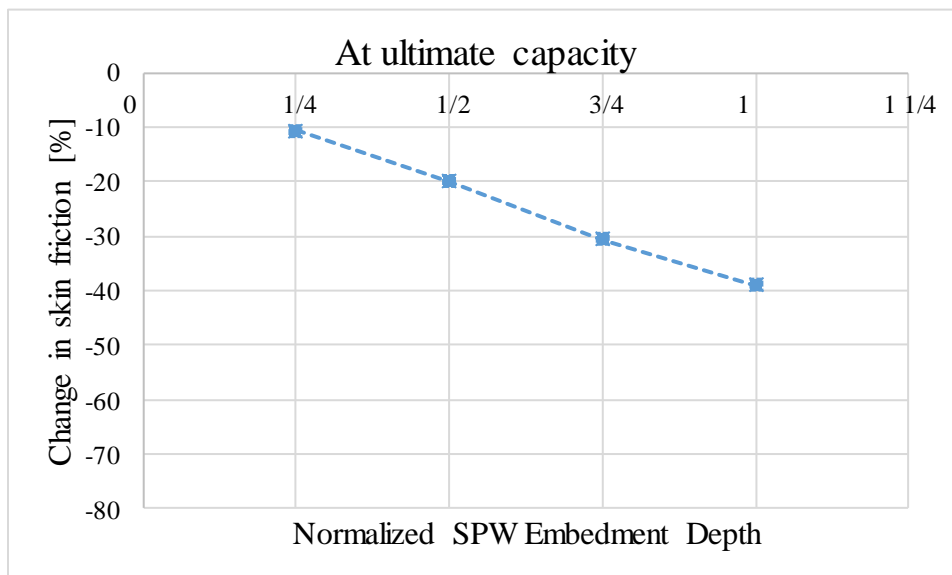


Figure 3.8 Change in skin friction component of total pile resistance at ultimate capacity for loading scenario 3 for different ratios of SPW embedment depth to pile embedment length

Table 3.2 Change in Davisson and ultimate capacity with respect to scenario 1, in terms of skin friction force.

Scenario 1		Davisson capacity		Ultimate capacity	
		34.20		107.13	
	Embedment depth ratio	Scenario 2	Scenario 3	Scenario 2	Scenario 3
Capacity	one-quarter	39.96	28.56	160.62	95.76
	one-half	45.02	23.82	180.92	85.68
	three-quarter	50.90	18.92	204.57	74.29
	full	54.02	11.53	217.11	65.30
% change in capacity	one-quarter	16.84	-16.49	49.93	-10.61
	one-half	31.63	-30.35	68.88	-20.02
	three-quarter	48.83	-44.68	90.95	-30.66
	full	57.96	-66.29	102.66	-39.05

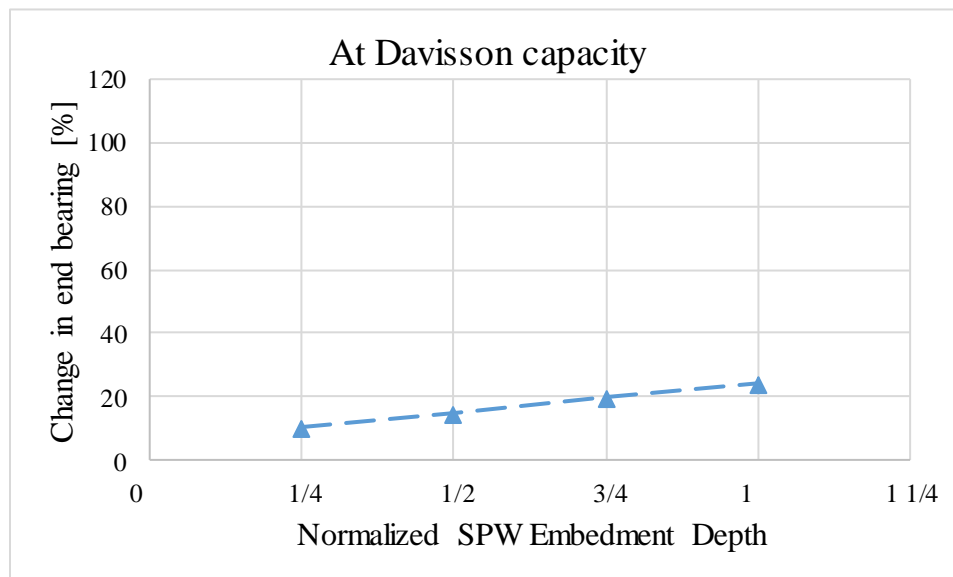


Figure 3.9 Change in end bearing component of total pile resistance at Davisson capacity for loading scenario 2 for different ratios of SPW embedment depth to pile embedment length

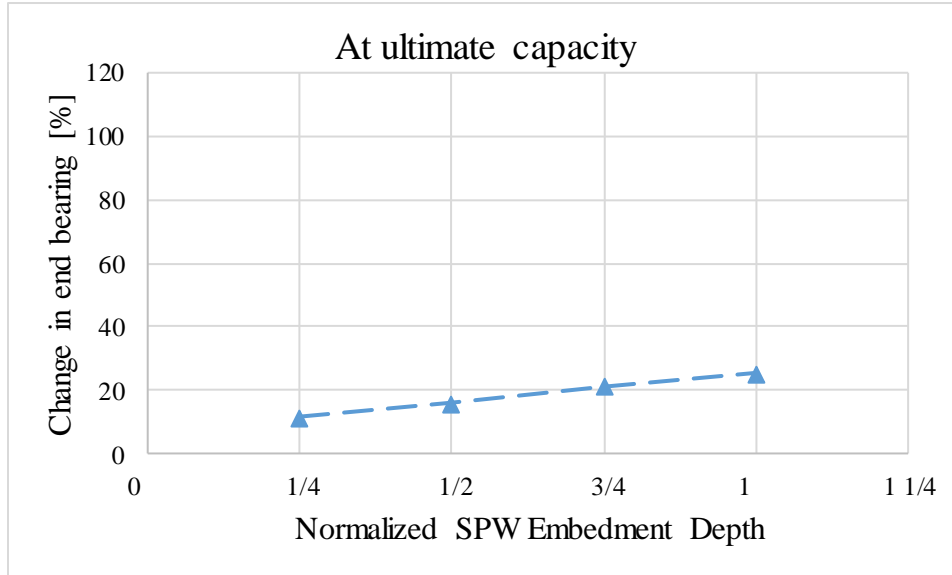


Figure 3.10 Change in end bearing component of total pile resistance at ultimate capacity for loading scenario 2 for different ratios of SPW embedment depth to pile embedment length

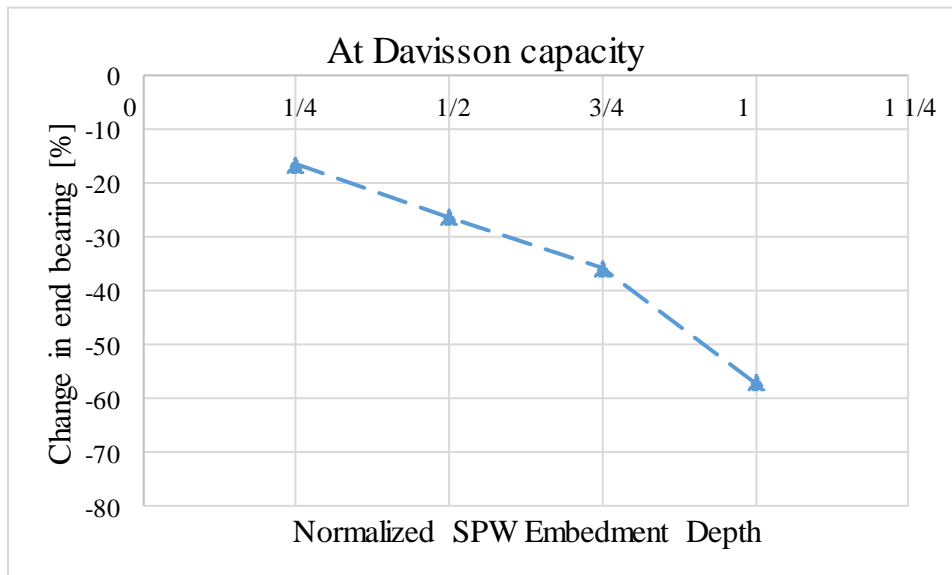


Figure 3.11 Change in end bearing component of total pile resistance at Davisson capacity for loading scenario 3 for different ratios of SPW embedment depth to pile embedment length

Finally, Figs. 3.9 and 3.10 show the increases in the end bearing component of total resistance which occur in scenario 2 for Davisson and ultimate capacities in terms of percentages. Figs. 3.11 and 3.12 show the corresponding reductions calculated for scenario 3. These values are listed in Table 3.3.

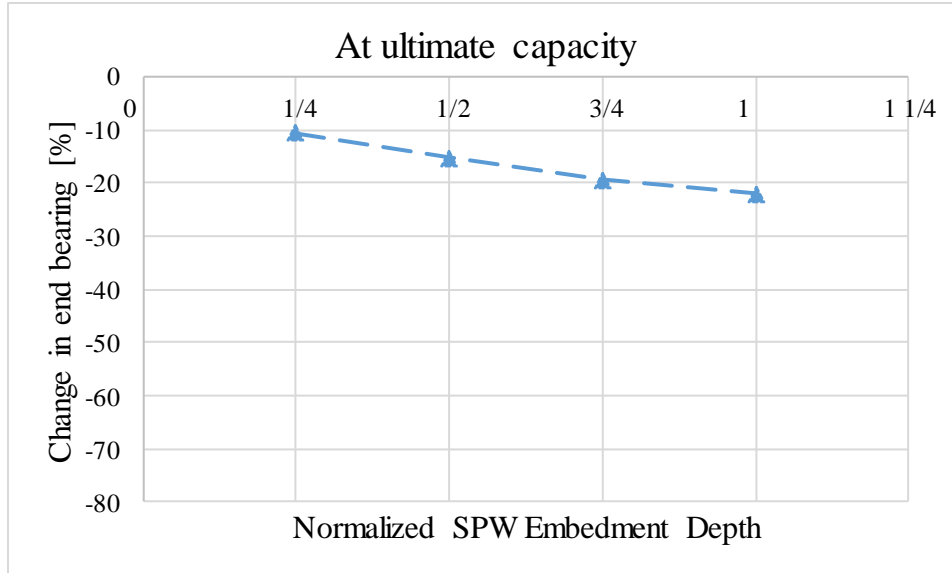


Figure 3.12 Change in end bearing component of total pile resistance at ultimate capacity for loading scenario 3 for different ratios of SPW embedment depth to pile embedment length

Table 3.3 Change in Davison and ultimate capacity with respect to scenario 1, in terms of end bearing force.

Scenario 1		Davison capacity		Ultimate capacity	
		117.80		368.97	
Capacity	Embedment depth ratio	Scenario 2	Scenario 3	Scenario 2	Scenario 3
	one-quarter	130.10	98.38	522.87	329.93
	one-half	135.06	86.96	542.77	312.83
	three-quarter	141.18	75.68	567.38	297.15
	full	146.06	50.78	587.00	287.67
% change in capacity	one-quarter	10.45	-16.49	11.72	-10.58
	one-half	14.65	-26.18	15.98	-15.22
	three-quarter	19.85	-35.76	21.24	-19.46
	full	23.99	-56.89	25.43	-22.03

3.3 Recommended Use of Graphical Design Tools

The plots given in Figs. 3.1 through 3.12, are recommended to be used as straightforward graphical tools for making quick assessments of total pile resistance and components of pile resistance upon pre-installation and post-removal of SPWs in close proximity to driven pile foundations. These plots also provide the construction engineer with basic guidance related to SPW behavior during installation and removal. An example is given below as a demonstration of using the design plots.

Let us consider a design problem in which a rectangular cofferdam is installed to a depth of 11.25 ft in medium dense FL sand. The square pile with width of 24 inches is then driven to a depth of 18 ft at a horizontal offset distance of 4 ft from the face of two SPWs constituting the cofferdam. The total pile Davisson and ultimate capacities of the single pile foundation are calculated, using the program FB-Deep, as 200 kips and 600 kips, respectively. The skin friction component of pile at Davisson and ultimate capacities was calculated as 42 kips and 175 kips respectively. The total load capacities after the removal of both the SPWs can be solved using Fig. 3.3 and Fig. 3.4; and the skin friction component after the removal of SPWs can be calculated using Figs. 3.7 and 3.8 to calculate the reduction factor to account for the effects of removal of SPWs in the design load capacities.

The ratio of SPW embedment depth to the pile embedment length is $11.25 \text{ ft} / 18 \text{ ft} = 0.625$. The horizontal offset distance between SPWS and pile is given as 4 ft. From Fig. 3.3, the reduction percentage is interpolated between the reduction percentage values of the embedment-depth ratios of 0.5 and 0.75; $\frac{0.625 - 0.5}{0.75 - 0.5} \times (37.76\% - 19.39\%) + 19.39\% = 28.57\%$. Thus, reduced Davisson pile capacity (DC) is estimated as

$$\begin{aligned} \text{Total pile resistance at DC on removal of SPWs} &= 200 \text{ kips} - \frac{28.57}{100} (200 \text{ kips}) \\ &= 200 - 57.15 = 142.85 \text{ kips} \end{aligned}$$

In a similar manner, the reduction in ultimate capacity is estimated using Fig. 3.4. The reduction percentage is interpolated between the reduction percentage values of the embedment depth ratios of 0.5 and 0.75: $\frac{0.625 - 0.5}{0.75 - 0.5} \times (20.63\% - 14.85\%) + 14.85\% = 17.74\%$. Thus, reduced ultimate capacity (UC) is estimated as:

$$\begin{aligned} \text{Total pile resistance at UC on removal of SPWs} &= 600 \text{ kips} - \frac{17.74}{100} (600 \text{ kips}) \\ &= 600 - 106.44 = 493.56 \text{ kips} \end{aligned}$$

The same procedure can be used to find the reduction in skin friction using Figs. 3.7 and 3.8. Thus, the reduction percentage is interpolated as:

$\frac{0.625 - 0.5}{0.75 - 0.5} \times (44.68\% - 30.35\%) + 30.35\% = 37.52\%$. The skin friction at Davisson capacity is calculated as:

$$\begin{aligned} \text{Skin friction at DC on removal of SPWs} &= 42 \text{ kips} - \frac{37.52}{100}(42 \text{ kips}) \\ &= 42 - 15.75 = 26.25 \text{ kips} \end{aligned}$$

For skin friction at ultimate capacity, the percentage reduction is calculated from Fig. 3.8 as:

$\frac{0.625 - 0.5}{0.75 - 0.5} \times (30.66\% - 20.02\%) + 20.02\% = 25.34\%$. The skin friction at ultimate capacity is calculated as:

$$\begin{aligned} \text{Skin friction at UC on removal of SPWs} &= 175 \text{ kips} - \frac{25.34}{100}(175 \text{ kips}) \\ &= 175 - 44.35 = 130.65 \text{ kips} \end{aligned}$$

CHAPTER 4 SUMMARY AND CONCLUSIONS

4.1 Summary Regarding Work Completed Toward Phase 2

The current task has been undertaken to provide geotechnical engineers with design-oriented graphical tools for use in determining pile design loads subject to the post removal of nearby SPW structures. Using the same techniques as in Phase 1 of this project, a three-dimensional discrete element method was carried out for assessments of granular soil behaviors under static and dynamic loading regimes. The interaction of the numerical soil assembly with structural components during the installation and removal of the SPW cofferdam structure, along with the dynamic pile driving process, have been explicitly modelled for the purpose of providing design recommendations. This task report extends the results and design tools presented in Phase 1, Task 5 (Chung et al. 2018c), to the case where the structural pile is driven in the proximity of the corner of a rectangular SPW cofferdam structure.

The study shows that the geometric configuration of pile-soil-SPW system has direct impact on the end bearing of the displacement pile foundations. The present analysis involves the identification of certain geometric parameters of the pile-soil-SPW arrangement that have the most influence on resistance offered by granular media to pile penetration. In order to facilitate the application of the results to engineering design problems, the numerical analysis is performed for three distinct physical scenarios: (1) pile driven into sand, followed by pile top-down load test; (2) two SPWs driven into sand one at a time in a cofferdam configuration, followed by pile driven into sand, ending with pile top-down load test; and (3) two SPWs driven into sand one at a time in a cofferdam configuration, followed by pile driven into sand, SPW removal one at a time in a reverse sequence, ending with pile top-down load test.

In summary, the discrete element analyses demonstrate that the actual deformation pattern associated with SPW installation and subsequent pile driving may be well simulated, and possibly differs from that assumed in existing continuum mechanics or cavity-expansion theory. The pile dynamic resistance is affected by deformation properties such as effective shear modulus and inter-granular friction coefficient, which ultimately produce the angle of dilation due to dynamic compaction. The Phase 2 results show strong dependence of pile capacity on the presence and geometric configuration of adjacent SPWs.

4.2 Conclusions

The results determined here for the pile-soil-SPW system are qualitatively similar to those obtained in Phase 1 for systems with a single SPW. A pile loaded in the presence of the cofferdam system (scenario 2) shows an increase in both Davisson and ultimate capacities. This extra bearing capacity is shown to increase with the embedment depth of the SPW cofferdam structure (Figs. 3.1 and 3.2). The presence of the SPWs has qualitatively similar but quantitatively differing effects on the skin friction and end bearing components of the total resistive force; while both increases with the depth of the nearby SPWs in scenario 2, Figs. 3.5 and 3.6 show that the percentage of skin friction increase is much larger than that of end bearing, shown in Figs. 3.9 and 3.10. This is due to the fact that the increase in resistance is due to the lateral confinement of the granular packing

by the SPWs, which ultimately has a stronger effect on the frictional resistance of the material on the driven pile.

Conversely, when the pile is loaded after the removal of a nearby SPW cofferdam (scenario 3), there is a marked reduction in bearing capacity when compared to a system in which no SPWs were present (i.e., scenario 1). In turn, the Davisson and ultimate capacities of the pile decrease further the deeper the SPW structure was embedded in the granular assembly (Figs. 3.3 and 3.4). The conclusions for the skin friction and end bearing components of total force also carry on to scenario 3, although with the opposite effect. Figs. 3.7 and 3.8 show that the resulting decrease in the skin friction component of resistance is larger than that which takes place in the end bearing component, shown in Figs. 3.11 and 3.12.

From the results presented in this report, it can be concluded that the number and geometrical arrangement of nearby SPWs has a pronounced effect on pile capacities – be it increase in pile capacity for loading scenario 2 or decrease in pile capacity for loading scenario 3. The resulting changes in capacity shown in the present study are all of larger magnitude than those presented in the Phase 1, Task 5 report for the case of one SPW only.

These patterns in the Davisson and ultimate capacities of a pile in scenarios 2 and 3 can be attributed to the local confinement, densities, and resistance of the numerical DSE assembly interacting with the SPW structure. When the SPW cofferdam is present during the pile loading, it resists that expansion of the soil body in response to the applied force. This in turn increases the effective confinement on the soil, which further resists the loaded pile, ultimately increasing its bearing capacity. However, when the SPW is removed prior to the loading of the pile, it creates a void in the granular assembly, which rearranges under its own body forces to compensate for the removal of the structural element. This in turn loosens the soil in the vicinity of the pile, decreasing its confining and resisting effects, ultimately leading to the reduction in loading capacity observed in the data. These effects are magnified in relation to the embedment depth of the SPW in relation to the pile, as a larger section of the granular assembly is effected in this way. The combined FEM-DEM numerical method may more accurately represent the responses of the granular assembly than traditional continuum-based methods. The results of Figs. 3.1-3.12 are intended to give practicing engineers a simple graphical way of quantifying these effects when facing relevant design decisions.

CHAPTER 5 REFERENCES

- Archard, J. F. (1957). "Elastic Deformation and the Laws of Friction," Proceedings of the Royal Society of London A, 243: pp.190-205
- Chung, J. H., McVay, M., Davidson, M., Taghavi, A., Nguyen, T., Taylor, A. (2018a). "Effect of Proximity of Sheet Pile Walls on the Apparent Capacity of Driven Displacement Piles, Task 4 Deliverable Report." University of Florida, Gainesville, FL.
- Chung, J. H., McVay, M., Davidson, M., Taghavi, A., Mishra, N., Zhang, Y., Nguyen, T. (2018b). "Effect of Proximity of Sheet Pile Walls on the Apparent Capacity of Driven Displacement Piles, Task 3.2 Deliverable Report." University of Florida, Gainesville, FL.
- Chung, J. H., McVay, M., Davidson, M., Taghavi, A., Mishra, N., Zhang, Y., Nguyen, T. (2018c). "Effect of Proximity of Sheet Pile Walls on the Apparent Capacity of Driven Displacement Piles, Task 5 Deliverable Report." University of Florida, Gainesville, FL.
- Greenwood, J.A. and Williamson, J.B.P., (1966). "Contact of Nominally Flat Surfaces", Proceedings of the Royal Society of London A., 295, pp. 300-319.